

# The kinematic similarity of two western boundary currents revealed by sustained high-resolution observations

Archer, M. R.<sup>1</sup>, S. R. Keating<sup>1</sup>, M. Roughan<sup>1,2,3</sup>,  
W. E. Johns<sup>4</sup>, R. Lumpkin<sup>5</sup>, F. Beron-Vera<sup>6</sup>, L. K. Shay<sup>4</sup>

Target Journal: *Geophysical Research Letters*

May 2018

<sup>1</sup>*School of Mathematics and Statistics, University of New South Wales (UNSW), Sydney, NSW 2052, Australia*

<sup>2</sup>*School of Biological Earth & Environmental Sciences, UNSW, Sydney, NSW 2052 Australia*

<sup>3</sup>*MetOcean Solutions (Meteorological Service of New Zealand)*

<sup>4</sup>*Department of Ocean Sciences, Rosenstiel School of Marine and Atmospheric Science (RSMAS), University of Miami, Florida 2049, USA*

<sup>5</sup>*Atlantic Oceanographic and Meteorological Laboratory, NOAA, Miami, Florida, USA*

<sup>6</sup>*Department of Atmospheric Sciences, RSMAS, University of Miami, Florida 2049, USA*

## Key points:

1. Multi-year surface velocity data of the Florida Current and East Australian Current are compared at 1km/1hr scales with high frequency radar
2. Despite contrasting local wind, bathymetry and meandering, the time-mean structure of their jet speed and lateral shear are almost identical
3. Eddy kinetic energy submesoscale wavenumber spectra are steep, with weak seasonal variability across both upstream western boundary currents

## Abstract

Western boundary currents (WBCs) modulate the global climate and dominate regional ocean dynamics. However, detailed inter-comparisons of the kinematic structure of WBCs have been hindered by a lack of sustained observational datasets. Here we compare multi-year, high-resolution observations (1km, hourly) of surface currents in two WBCs (Florida Current and East Australian Current) upstream of their separation point. Current variability is dominated by meandering, and the WBCs exhibit contrasting time-mean velocities in an Eulerian coordinate frame. By transforming to a jet-following coordinate frame, we find that the time-mean surface velocity structure of the WBC jets are remarkably similar, despite contrasting local wind, bathymetry, and meandering signal. Both WBCs show steep submesoscale kinetic energy wavenumber spectra with weak seasonal variability, in contrast to recent findings in other ocean regions. Our results suggest that it is the mesoscale flow field that controls mixing and ocean dynamics in these regions.

This article has been accepted for publication and undergone full peer review but has not been through the copyediting, typesetting, pagination and proofreading process which may lead to differences between this version and the Version of Record. Please cite this article as doi: 10.1029/2018GL078429

## 1. Introduction

Western boundary currents (WBCs) are warm, narrow and intense currents that flow poleward along the western edge of ocean basins, balancing the equatorward wind-driven transport in the open ocean. WBCs and their eddy field modulate Earth's climate by exporting heat from the tropics toward the poles, and mediate large air-sea heat and moisture fluxes that fuel mid-latitude storms [Yu and Weller, 2007]. They also act as a sink for carbon dioxide via subduction and biological uptake [Cronin et al., 2010; Ducklow et al., 2001]. At the regional level, WBCs play a critical role in shelf circulation and coastal ecology, mixing water masses and upwelling nutrients into the sunlit surface layers where they are utilized by ecological communities [Lee et al., 1981; Shulzitski et al., 2015] and commercial fisheries [Richardson et al., 2009].

Because of their importance, significant effort has been invested to monitor the structure and variability of WBCs [see review by Imawaki et al., 2013]. Such observational datasets provide insight into the influence of WBCs in both global and regional circulation, helping to constrain numerical ocean models. However, there are still many open questions, especially at scales of  $O(1-10)$  km that are highly relevant to the biogeochemistry and productivity of continental shelf regions [Mahadevan, 2016]. These scales, termed submesoscale, differ dynamically from larger mesoscale flows as they are (i) below the first baroclinic Rossby radius of deformation, (ii) exhibit vertical velocities as large as 100 m/day, and (iii) are associated with  $O(1)$  Rossby number ( $Ro=V/fl$ , where  $V$  is an rms velocity,  $f$  the local Coriolis frequency, and  $l$  the horizontal length scale), indicating the importance of advection in the force balance [McWilliams, 2016]. Recent observations reveal seasonality in the submesoscale flow field over the open ocean and WBC extensions [Callies et al., 2015; Qiu et al., 2017], with a more energetic submesoscale eddy kinetic energy (EKE) field during wintertime. As yet there have been no observational studies of submesoscale seasonality in WBCs upstream of their separation point, where the dynamics are strongly anisotropic and dominated by the presence of the jet [Schaeffer et al., 2017].

Here we make the first detailed comparison of two upstream WBCs – the Florida Current in the northern hemisphere, and the East Australian Current in the southern hemisphere – using multi-year observations of surface currents at hourly/kilometer scales from high frequency (HF) radar [Paduan & Washburn, 2013]. These complementary datasets offer unprecedented views of the two WBC jets as they flow along the eastern coastlines of the US and Australia, respectively. Whereas a mooring array typically resolves  $O(10)$  grid points in a cross-jet direction, HF radar resolves  $O(1)$ -km scale grid points over a range of 100 km in both cross-jet and along-jet directions. This high spatial resolution allows us to accurately track the jets as they meander across the continental slope, and resolve frontal eddies and other instabilities in 2D [e.g. Shay et al., 1998; Archer et al., 2015a; Schaeffer et al., 2017; Mantovanelli et al., 2017]. The two study regions are:

**i. The Florida Current (FC)** is the upstream branch of the Gulf Stream system that is constrained within the Florida Straits (*Fig. 1a*). It flows northward following the narrow continental shelf ( $\sim 3$  km offshore Miami) and exits the Straits at  $26^\circ\text{N}$ , continuing along the shelf until it separates from the coastline at Cape Hatteras ( $32^\circ\text{N}$ ). Around  $25^\circ\text{N}$  the FC's mean core speed is  $\sim 1.6 \text{ m s}^{-1}$  located 40 km offshore [Richardson et al., 1969; Archer et al., 2017a]. The FC has a volume transport of  $\sim 30 \text{ Sv}$  with a standard deviation (STD) of 3 Sv (1

Sverdrup =  $10^6 \text{ m}^3 \text{ s}^{-1}$ ) [Meinen et al., 2010]. It undergoes a weak seasonal cycle in speed and volume transport ( $\sim 10\%$  of observed variance), with a maximum most commonly observed during boreal summer [Meinen et al., 2010]. The FC exhibits largest variability at 2-30 days, due to local and regional wind stress, and lateral meandering with an amplitude of  $\sim 60$  km and STD of 8 km [Johns and Schott, 1987; Schott et al., 1988; Archer et al., 2017b]. Remote wind forcing, communicated via first mode baroclinic Rossby waves, has been shown to affect the annual cycle in volume transport [Domingues et al., 2016], but for the data presented here at  $25\text{-}26^\circ\text{N}$  the Bahamas island chain blocks most of this direct mid-ocean influence [Archer et al., 2017a].

**ii. The East Australian Current (EAC)** closes the South Pacific subtropical gyre, flowing poleward along SE Australia (*Fig. 1b*). At  $30^\circ\text{S}$  the EAC flows over the continental slope about 30 km offshore. In contrast to the Gulf Stream, the EAC does not have one dominant separation region controlled by coastline geometry. Instead, the separation point ranges from  $28\text{-}37^\circ\text{S}$ , but  $30\text{-}32^\circ\text{S}$  about 50% of the time [Cetina-Heredia et al., 2014]. At  $30\text{-}31^\circ\text{S}$ , the EAC has a mean core speed between  $0.6\text{-}1.35 \text{ m s}^{-1}$  [Mata et al., 2000; Schaeffer et al., 2017; Archer et al., 2017b], and a volume transport of  $\sim 22 \text{ Sv}$  with a STD of  $\sim 5\text{-}7 \text{ Sv}$  [Mata et al., 2000; Sloyan et al., 2016]. The jet speed and EKE undergo a seasonal cycle with an austral summer maximum [Ridgway & Godfrey, 1997; Archer et al., 2017b]. The EAC meanders with a longer period than the FC, at 20-45 days, with a second dominant mode at 65-110 days associated with mesoscale eddy variability of the separation point [Mata et al., 2000; Bowen et al., 2005]. The amplitude of EAC meandering is larger than the FC, with a lateral displacement from the mean over 80 km and STD of 20 km [Archer et al., 2017b]. Local wind forcing can drive sporadic upwelling and cross shelf transport in the EAC, but generally current variability occurs on longer timescales, and is largely unrelated to local winds (e.g. Schaeffer et al. [2014], their Figure 10). Regional wind forcing can influence the timing of the EAC eddy shedding events, while remote wind forcing has limited impact on the intrinsically variable EAC system [Bull et al., 2017].

## 2. Data and Methods

Both WBCs were monitored with WERA phased-array HF radar systems [Gurgel et al., 1999; Shay et al., 2007]. In the FC (*Fig. 1a,c*), two years of data (Jan 2005 – Dec 2006) are analyzed from two sites (Miami and Key Largo), operating at 16.045 MHz [Shay et al., 2008; Martinez-Pedraja et al., 2013]. Vector velocities on a Cartesian 1.2 km resolution grid are calculated from quality controlled radials every 20 min with the unweighted least-squares method of Gurgel et al. [1994]. To quality control the radial data, each grid point timeseries is smoothed with a 9-point (3 hour) Hann window. Data points exceeding 3 STD from a running 5 day mean and grid points with a STD over  $0.5 \text{ m s}^{-1}$ , or with less than 15% data coverage, are not included in the analysis [Archer et al., 2015b]. This dataset is discussed in detail by Archer et al. [2017a].

In the EAC (*Fig. 1b,d*), four years of HF radar data (Mar 2012 - Jul 2016) are analyzed from two sites operating at 13.92 MHz near Coffs Harbour ( $30\text{-}31^\circ\text{S}$ ), deployed as part of Australia's Integrated Marine Observing System (IMOS) [Roughan et al., 2015; Wyatt et al., 2017]. Each radial velocity dataset is combined using the unweighted least-squares method of Gurgel et al. [1994] to a Cartesian grid with 1.5 km resolution at 10 min intervals smoothed

with a 17-point (3 hour) Hann window. The timeseries is de-spiked by removing occurrences of consecutive data points separated by  $0.8 \text{ m s}^{-1}$ , and outliers over 3 STD from a 7-day mean and 3.5 STD from the total mean were removed. Full details are presented in Archer et al. [2017b].

Subsurface current data from the EAC is obtained from a bottom-mounted ADCP deployed at the 100 m isobath (named CH100), within the HF radar footprint at  $30.27^\circ\text{S}$  (*Fig. 1d*) [Schaeffer et al., 2013]. Current velocity is measured at 4 m bin resolution between 13-89 m, every 5 minutes, and subsampled to 3 hours to match the HF radar data. Concomitant subsurface velocity data are not available for the FC.

Wind data in the Florida Straits is measured at Fowey Rocks meteorological station, 8 km offshore Miami's Biscayne Bay (*Fig. 1c*). In southeast Australia, wind measurements are taken from Coffs Harbour meteorological station (*Fig. 1d*). Both datasets are subsampled to 3 hours to match HF radar measurements [Archer et al., 2017a,b].

To control for meandering, HF radar data for each region were converted to a time-evolving jet coordinate frame [Archer et al., 2017a,b]. In jet coordinates the position of the jet core is the origin of reference rather than a geographical location [Halkin and Rossby, 1985]. In this frame, a time-mean representation of the jet is not contaminated by smearing of the meandering high velocity core, so higher core speeds and lateral shears are retained. Eddy velocities are given by  $u' = u - \bar{u}$ , where  $u$  and  $\bar{u}$  are the instantaneous and time mean currents in the jet coordinate frame, respectively. The eddy kinetic energy in the jet frame is  $EKE = 0.5 \times (u'^2 + v'^2)$ .

EKE wavenumber power spectra are calculated over a subset of longitudinal (geographical frame) or cross-jet (jet frame) transects, for coverage  $>75\%$ . Depending on time-variable data coverage, these transects are generally 30-70 km long, with a resolution of 1.2 km for the FC (1.5 km for the EAC). For each transect, data is linearly detrended, the time and space mean profile is subtracted, a Hann window is applied, and the Fourier transform calculated. The time mean is taken over the full observation record; we tested the sensitivity of different time windows (7d, 30d, seasonal), and found the variation does not significantly impact the mean wavenumber slopes. We average spectra over summer and winter. Summer (winter) is defined for the FC (EAC) as June-July-August, and winter (summer) is December-January-February. Frequency spectra are calculated only in geographical coordinates, since gaps are larger and more frequent in the jet coordinate timeseries (usually caused by insufficient data during the coordinate conversion). Spectral confidence levels were calculated using a  $\chi^2$ -distribution (see Supporting Information).

### 3. Observations

#### Mean jet profiles

In geographical coordinates, the two WBCs have contrasting cross-jet profiles of mean speed (*Fig. 2a*). The FC mean core speed is  $1.5 \text{ m s}^{-1}$  with STD of  $0.35 \text{ m s}^{-1}$ . In contrast, the EAC profile is broader and more diffuse, with mean core speed of  $0.8 \text{ m s}^{-1}$  and STD of  $1.1 \text{ m s}^{-1}$ . The velocity shear in the FC is twice that in the EAC, although both WBCs exhibit similar asymmetry in magnitude of cyclonic to anticyclonic shear (*Fig. 2b*), as previously observed in the Gulf Stream [e.g. Rossby and Zhang, 2001].

In jet coordinates, the mean cross-jet velocity profile of the FC and EAC converge, with core speeds of 1.6 and 1.35 m s<sup>-1</sup>, and STDs reduced to 0.2 and 0.3 m s<sup>-1</sup>, respectively (*Fig. 2c*). Even more striking is the similarity in the two jet's time-mean lateral shear profiles, which are almost identical (*Fig. 2d*). The remaining difference in speed may be due to the FC carrying a component of the thermohaline circulation, with larger observed volume transport than the EAC, together with the spatial constraint of the relatively narrow and shallow Florida Straits. Differences in shear outside the core are also primarily because the FC is restricted by land on both sides, so anticyclonic shear must remain relatively large for  $v$  to reduce to zero at the Bahamas (*Fig. 1a*). In contrast, the EAC has no bathymetric constraint east of the jet, so anticyclonic shear weakens toward zero with increasing distance from the core.

### **Temporal variability of currents**

Surface current velocity fields of the EAC and FC exhibit similar power density spectral slopes of kinetic energy (KE), with a distinct peak at the principal lunar semidiurnal M<sub>2</sub> and a broader peak at the diurnal K<sub>1</sub> and O<sub>1</sub> frequencies (*Fig. 3c,d*). In the EAC at 30.5°S the inertial period is 23.6 hours, in the FC at 25.5°N it is 27.9 hours, hence the broadband diurnal peak that contains near-inertial wave signals [Shay et al., 1998; Archer et al., 2015a]. In these high geostrophic shear regions, near-inertial period motions can be shifted by the background vorticity so that they are closer to the diurnal period [e.g. Kunze & Toole, 1997]. The critical latitude (at 30°N and S for no background vorticity) is where the local inertial period is close to diurnal forcing driven by tides and the land-sea breeze [e.g. Simpson et al., 2002; Kim & Crawford, 2014; Mihanović et al., 2016]. Because of this, both datasets exhibit strong diurnal variability. However, in the mesoscale frequency range the EAC exhibits much higher variability, associated with a more energetic meandering signal in both space (amplitude shown in the 2D histograms of *Fig. 1c,d*) and time (*Fig. 3e*).

Seasonality in KE variance is similar for both WBCs (*Fig. 3c,d*), with a clear summer intensification near the diurnal period, corresponding to the stronger summer land/sea breeze (*Fig. 3a,b*). For periods up to ~10 days wind forcing may still be the primary driver of current fluctuations; the FC exhibits more variability during winter and the EAC during summer, which matches local wind variability. For periods longer than ~10 days, summer variance is larger than winter, in contrast to local wind. In the EAC, near-bottom ocean currents measured at mooring CH100 (*Fig. 1d*) do not show any seasonal change in energy across the internal wave band, with the exception of diurnal and semi-diurnal peaks, which are larger during winter (*Fig. 3f*). This contrasts with both the surface currents and the summer peak in wind forcing, suggesting that surface currents exhibit seasonal wind-driven fluctuations not observed near the bottom. At periods above 10 days, surface and near-bottom currents exhibit the same summer intensification, in direct contrast to wind forcing, suggesting an internal ocean signal not driven by the local wind [Schaeffer et al., 2014].

### **Spatial variability of currents**

Wavenumber spectra in geographical coordinates contain more energy than in jet coordinates at the larger scales (>~15 km), and less at the smaller scales (<~15km), although the mean slopes are not substantially different between coordinate frames (*Fig. 4*). This is because the geographical time-mean, which is used to obtain the fluctuating flow field, has spread the

energy of the jet in space (*Fig. 2a*), leading to higher variability at the larger scales, and less at small scales.

In jet coordinates, mean EKE wavenumber spectral slopes are -2.6 in the FC, and -3.2 in the EAC (*Fig. 4*). The steeper EAC slope is due to higher variability in the mesoscale range ( $> 15$  km [Schaeffer et al., 2014]). Even though we control for lateral movement of the WBCs in jet coordinates, there are still structural variations due to meandering and associated eddying that influence the spectra. Spectra of divergent motions were weak in both WBC regions (not shown), where flow is dominated by the rotational component. In both WBCs, there is weak seasonality at submesoscales, and only in the FC is there a marginal winter increase in variance above  $\sim 15$  km.

#### 4. Discussion

Whereas previous studies qualitatively compared WBCs [e.g. Szabo & Weatherly, 1979] this is the first time that two WBCs have been examined using analogous datasets in an objective frame of reference that controls for the meandering signal. By converting to a jet-following coordinate frame, we find the time-mean velocity and shear profiles of the two WBC jets are remarkably similar. Rossby and Zhang [2001] showed the Gulf Stream velocity profile near  $70^\circ\text{W}$  can be modeled with two back-to-back exponentials, which have scale-widths of comparable length to the Rossby radius of deformation set by the depth of the pycnocline. We fitted an exponential function to the cyclonic shear region of the velocity profiles (*Fig. 2c*; ignoring 10 km about the rounded jet core), obtaining scale-widths of 24 km and 16 km in the FC and EAC, respectively. These scale-widths match quite well existing observations of Rossby deformation radii in the cyclonic shear region of the WBCs;  $\sim 15$ -30 km in the Florida Straits [Shay et al., 2000], and  $\sim 15$  km in the Tasman Sea [Schaeffer et al., 2014].

Nonetheless, differences still exist between the two WBCs. The EAC has a more energetic eddy field, evident in the frequency and wavenumber spectra (*Fig. 3 and 4*). This is at least partly due to contrasting coastlines: at  $25^\circ\text{N}$ , the FC is constrained within a channel and unable to sustain large meanders, and mesoscale eddies that form upstream are sheared apart as they are advected through the narrowing and shoaling channel [Frantantoni et al., 1998]. In contrast, the EAC is unimpeded to the east, and susceptible to large-amplitude displacements offshore by the advection of mesoscale cyclonic eddies along its inshore flank [Roughan et al., 2017]. Indeed, the EAC system is unique among WBCs for its large EKE-to-KE ratio [Boland & Hamon, 1970; Godfrey et al., 1980].

Both upstream WBC regions exhibit an approximate  $k^{-3}$  power law in the EKE wavenumber spectra. The observed slopes are similar to those reported by Callies & Ferrari [2013] in the Gulf Stream extension but steeper than in the Kuroshio ( $k^{-2.3}$ ; Qiu et al. [2017]) and in the subtropical North Pacific ( $k^{-2}$ ; Callies & Ferrari [2013]). From a global survey of mesoscale wavenumber spectra, Xu & Fu [2011] showed the steepest slopes are over WBC regions. In the coastal ocean, Lekien & Coulliette [2007] found  $k^{-3}$  using HF radar in Monterey Bay, and Soh et al. [2018] found  $k^{-2}$  to  $k^{-3}$  from HF radar offshore San Diego. Results from a global analysis of drifter pair separation by Corrado et al. [2017] also found steep slopes down into the marginal submesoscale range (5 km). Caution should be taken when attempting to reconcile wavenumber slopes to turbulence theory [Armi & Flament, 1985]; however, our results are consistent with quasigeostrophy [Charney, 1971], implying ocean dynamics and

mixing in these regions are controlled by the large-scale flow [Beron-Vera & Olascoaga, 2009; Beron-Vera & LaCasce, 2016].

In both WBCs, current variability peaks during summer at periods  $>10$  days, in contrast to local wind forcing (*Fig. 3a,b*). Increased summer EKE has been observed before in WBCs [e.g. Ridgway & Godfrey, 1997; Qiu et al., 2004; Archer et al., 2017b], in phase with summer intensification of WBC jet speeds [Archer et al., 2017b]. The reason for an observed global EKE summer maximum is still debated. The prevailing theory is that seasonal changes in upper ocean stratification modulate baroclinic instability [Gill et al., 1974], which is greatest in spring when the meridional thermocline tilt is maximum [Qiu et al., 1999; Capet et al., 2016]. Subsequent summer heating and reduced wind-driven vertical mixing flattens the thermocline, releasing available potential energy in the form of EKE [Kang & Curchitser, 2013], with a phase lag controlled by the growth rate of baroclinic mesoscale eddies [Qiu, 1999]. Other proposed mechanisms include seasonal changes in dissipation, rather than production, of EKE [Duhaut and Straub, 2006].

We do not observe a distinct seasonal cycle in EKE wavenumber spectra, in contrast to recent studies that show higher energy within the submesoscale range during winter [Qiu et al., 2017; Callies et al., 2015]. Submesoscale motions have a variety of generation mechanisms including mixed layer instability (MLI), direct wind forcing, or Charney instability, all of which are sensitive to surface mixing and hence show a seasonal dependence [McWilliams, 2016]. However, submesoscales are also generated from frontogenesis by a mesoscale straining field or interactions with topography, which don't have any seasonal dependence. The studies above focused on open ocean areas where the mean current flow is weaker and MLIs strengthen in winter with greater mixed layer depth (MLD). Here we resolve strong upstream WBC jets against the continental slope that undergo a weaker MLD seasonal cycle [Gula et al., 2014], with submesoscale frontal instabilities that are related to topographic interaction [Gula et al., 2015] and exhibit no seasonal cycle [Lee and Mayer, 1977; Schaeffer et al., 2017]. Weak submesoscale seasonality has also been documented by Yoo et al. [2018] on the east coast of Korea, which they attribute to the formation mechanism being mesoscale frontogenesis and topographic shear.

While this study represents the first detailed investigation of kinematic similarities between two WBCs, we are unable to investigate the underlying dynamics with only surface observations. Nonetheless, these observed commonalities can inform ocean models that resolve these features. Looking forward, we need more concurrent surface and sub-surface observations to measure how WBC are changing on inter-annual to decadal timescales.

## Acknowledgments

We thank two reviewers whose comments improved the quality of the paper. US HF radar data are available from the US National HF Radar Network (<http://cordc.ucsd.edu/projects/mapping/maps/> and <http://iwave.rsmas.miami.edu/wera/>), and Fowey Rocks wind data from <http://www.ndbc.noaa.gov/>. Thanks to Jorge Martinez-Pedraja who maintains the Florida sites. Australian HF radar and mooring datasets are available through IMOS (<http://imos.aodn.org.au/imos>), and wind data from the Bureau of Meteorology (<http://www.bom.gov.au/>). IMOS is supported by the Australian Government through the National Collaborative Research Infrastructure Strategy and the Super Science Initiative. We thank IMOS Ocean Radar Facility for HF radar maintenance and data management. SK was supported by UNSW Silverstar Research Grant. RL was funded by the Atlantic Oceanographic and Meteorological Laboratory and Ocean Observation and Monitoring division of NOAA. FJBV was supported by the Gulf of Mexico Research Initiative as part of the Consortium for Advanced Research on Transport of Hydrocarbon in the Environment. LKS gratefully acknowledges support by NOAA IOOS-supported South East Coastal Ocean Observing Regional Association through grants NA11NOS0120033 and NA16NOS0120028.

## Supporting Information

### Conversion to Jet Coordinates

The jet core is identified within each 2D current map as the ridge of maximum current speed from south to north for the FC (and vice versa for the EAC). For each jet core grid point identified along the ridge, a straight line of grid points running orthogonally through it constitutes the cross-jet transect. For every grid point along the cross-jet transect, we calculate distance to the core and rotate  $u/v$  components to cross-stream/downstream based on the jet core direction. All cross-jet transects are placed in a new coordinate system with an x-axis (*distance-to-core*, centered on zero and interpolated to 1.5 km spacing) and a y-axis (*jet core latitude*, where cross-jet grid points may have any original latitude). Refer to Archer et al. [2017a] for a full description of the coordinate conversion method with HF radar data.

### Calculation of Confidence Levels in Wavenumber Spectra

HF radar data provides a large number of transects (time and space) over which to calculate spectra. For example, in the FC jet frame there are 53,759/32,882 spectra in summer/winter (34,000/66,198 in the EAC). For confidence intervals, we assume a  $\chi^2$ -distribution, and use equivalent degrees of freedom (DOF) based on block averaging spectra from all transects over time, after taking into account integral timescales of the ocean currents in the FC (EAC) of 6 days (8 days), calculated via Equation 5.16 of Emery and Thomson [1998]. We conservatively assume all transects within one HF radar map are not independent, so do not count them in the DOF calculation. Because spatial coverage varies (and hence spectral resolution), the spectra are band averaged over 2 frequency bins. This leads to a DOF of  $2 \times (8/3) \times N/T^*$ , where  $N$  is the length of the timeseries,  $T^*$  is the integral timescale, and the factor of  $8/3$  takes into account the effect of the Hann window [Emery and Thomson, 1998].

## References

- Archer, M. R., L. K. Shay, B. Jaimes, & J. Martinez-Pedraja, (2015a). Observing frontal instabilities of the Florida Current using high frequency radar, In: Coastal Ocean Observing Systems, Liu, Y., H. Kerkering, R. H. Weisberg, eds. Elsevier. doi:10.1016/B978-0-12-802022-7.00011-0
- Archer, M. R., Shay, L. K., and Martinez-Pedraja, J. (2015b). Evaluation of WERA HF Radar Observations: Currents, Winds and Waves. In Current, Waves and Turbulence Measurements (CWTM), 2015 IEEE/OES 11th (pp. 1-9). doi: 10.1109/CWTM.2015.7098148.
- Archer, M. R., Shay, L. K., & Johns, W. E. (2017a). The surface velocity structure of the Florida Current in a jet coordinate frame. *Journal of Geophysical Research: Oceans*, 122, 9189–208. doi.org/10.1002/2017JC013286
- Archer, M. R., Roughan, M., Keating, S. R., & Schaeffer, A. (2017b). On the variability of the East Australian Current: Jet structure, meandering, and influence on shelf circulation. *Journal of Geophysical Research: Oceans*, 122, https://doi.org/10.1002/2017JC013097.
- Armi, L., and P. Flament (1985), Cautionary remarks on the spectral interpretation of turbulent flows, *J. Geophys. Res.*, 90(C6), 11779–11782, doi:10.1029/JC090iC06p11779
- Beron-Vera, F. J., & Olascoaga, M. J. (2009). An assessment of the importance of chaotic stirring and turbulent mixing on the West Florida Shelf. *Journal of physical oceanography*, 39(7), 1743-1755, <https://doi.org/10.1175/2009JPO4046.1>
- Beron-Vera, F. J., & LaCasce, J. H. (2016). Statistics of simulated and observed pair separations in the Gulf of Mexico. *Journal of Physical Oceanography*, 46(7), 2183-2199. <https://doi.org/10.1175/JPO-D-15-0127.1>
- Boland, F. M., & Hamon, B. V. (1970, August). The East Australian Current, 1965–1968. In *Deep Sea Research and Oceanographic Abstracts* (Vol. 17, No. 4, pp. 777-794). Elsevier, [https://doi.org/10.1016/0011-7471\(70\)90041-0](https://doi.org/10.1016/0011-7471(70)90041-0)
- Bowen, M. M., Wilkin, J. L., and Emery, W. J. (2005). Variability and forcing of the East Australian Current. *Journal of Geophysical Research: Oceans*, 110(C3), C03019, doi:10.1029/2004JC002533
- Bull, C., Kiss, A. E., Jourdain, N. C., England, M. H., & van Sebille, E. (2017). Wind Forced Variability in Eddy Formation, Eddy Shedding, and the Separation of the East Australian Current. *Journal of Geophysical Research: Oceans*. <https://doi.org/10.1002/2017JC013311>
- Callies, J., and Ferrari, R. (2013). Interpreting energy and tracer spectra of upper-ocean turbulence in the submesoscale range (1–200 km). *Journal of Physical Oceanography*, 43(11), 2456-2474, <https://doi.org/10.1175/JPO-D-13-063.1>
- Callies, J., Ferrari, R., Klymak, J. M., and Gula, J. (2015). Seasonality in submesoscale turbulence. *Nature communications*, 6:6862 doi: 10.1038/ncomms7862.
- Capet X, Roulet G, Klein P, Maze G (2016) Intensification of upper ocean submesoscale turbulence through Charney baroclinic instability. *J Phys Oceanogr* 46(11):3365–3384, <https://doi.org/10.1175/JPO-D-16-0050.1>
- Cetina-Heredia, P., Roughan, M., Van Sebille, E., and Coleman, M. A. (2014). Long-term trends in the East Australian Current separation latitude and eddy driven transport. *Journal of Geophysical Research: Oceans*, 119(7), 4351-4366, doi:10.1002/2014JC010071
- Charney, J. G. (1971). Geostrophic turbulence. *Journal of the Atmospheric Sciences*, 28(6), 1087-1095.
- Corrado, R., Lacorata, G., Palatella, L., Santoleri, R., & Zambianchi, E. (2017). General characteristics of relative dispersion in the ocean. *Scientific reports*, 7, 46291. doi:10.1038/srep46291
- Cronin, M.F., N. Bond, J. Booth, H. Ichikawa, T.M. Joyce, K. Kelly, M. Kubota, B. Qiu, C. Reason, M. Rouault, C. Sabine, T. Saino, J. Small, T. Suga, L.D. Talley, L. Thompson, and R.A. Weller, 2010: Monitoring ocean-atmosphere interactions in western boundary current extensions. In *Proceedings of OceanObs'09: Sustained Ocean Observations and Information for Society, Venice, Italy, September 2009*. J. Hall, D.E. Harrison, and D. Stammer, Eds., ESA Publication WPP-306, vol. 2, pp. 21-25, doi:10.5270/OceanObs09.cwp.20.

- Duhaut, T. H., & Straub, D. N. (2006). Wind stress dependence on ocean surface velocity: Implications for mechanical energy input to ocean circulation. *Journal of physical oceanography*, 36(2), 202-211, <https://doi.org/10.1175/JPO2842.1>
- Domingues, R., M. Baringer, and G. Goni (2016). Remote sources for year-to-year changes in the seasonality of the Florida Current transport, *J. Geophys. Res. Oceans*, 121, 7547–7559, doi:10.1002/2016JC012070.
- Ducklow, H. W., Steinberg, D. K., & Buesseler, K. O. (2001). Upper ocean carbon export and the biological pump. *OCEANOGRAPHY-WASHINGTON DC-OCEANOGRAPHY SOCIETY-*, 14(4), 50-58, <http://dx.doi.org/10.5670/oceanog.2001.06>
- Emery, W. J., and Thomson, R. E. (1998). Data analysis in physical oceanography. Pergamon.
- Fratantoni, P. S., Lee, T. N., Podesta, G. P., and Muller-Karger, F. (1998). The influence of Loop Current perturbations on the formation and evolution of Tortugas eddies in the southern Straits of Florida. *Journal of Geophysical Research: Oceans*, 103(C11), 24759-24779, doi:10.1029/98JC02147.
- Gill, A. E., Green, J. S. A., & Simmons, A. J. (1974). Energy partition in the large-scale ocean circulation and the production of mid-ocean eddies. In *Deep Sea Research and Oceanographic Abstracts* (Vol. 21, No. 7, pp. 499-528). Elsevier. [https://doi.org/10.1016/0011-7471\(74\)90010-2](https://doi.org/10.1016/0011-7471(74)90010-2)
- Godfrey, J. S., Cresswell, G. R., Golding, T. J., Pearce, A. F., and Boyd, R. (1980). The separation of the east Australian current. *Journal of Physical Oceanography*, 10(3), 430-440, [https://doi.org/10.1175/1520-0485\(1980\)010<0430:TSOTEA>2.0.CO;2](https://doi.org/10.1175/1520-0485(1980)010<0430:TSOTEA>2.0.CO;2)
- Gula, J., Molemaker, M. J., & McWilliams, J. C. (2014). Submesoscale cold filaments in the Gulf Stream. *Journal of Physical Oceanography*, 44(10), 2617-2643. <https://doi.org/10.1175/JPO-D-14-0029.1>
- Gula, J., M. J. Molemaker, and J. C. McWilliams (2015), Topographic vorticity generation, submesoscale instability and vortex street formation in the Gulf Stream. *Geophys. Res. Lett.*, 42, 4054–4062. doi: 10.1002/2015GL063731.
- Gurgel, K. W. (1994). Shipborne measurement of surface current fields by HF radar. In *OCEANS'94. 'Oceans Engineering for Today's Technology and Tomorrow's Preservation.' Proceedings* (Vol. 3, pp. III-23). IEEE.
- Gurgel, K. W., Antonischki, G., Essen, H. H., and Schlick, T. (1999). Wellen Radar (WERA): a new ground-wave HF radar for ocean remote sensing. *Coastal Engineering*, 37(3), 219-234.
- Halkin, D., and Rossby, T. (1985). The structure and transport of the Gulf Stream at 73 W. *Journal of Physical Oceanography*, 15(11), 1439-1452, [https://doi.org/10.1175/1520-0485\(1985\)015<1439:TSATOT>2.0.CO;2](https://doi.org/10.1175/1520-0485(1985)015<1439:TSATOT>2.0.CO;2).
- Imawaki S, Bower A, Beal L, Qiu B. 2013. Western boundary currents. In: *Ocean Circulation and Climate: A 21st Century Perspective*, ed. G Siedler, SM Griffies, J Gould, JA Church, pp. 305–38. Oxford, UK: 2nd ed.
- Johns, W. E., and Schott, F. (1987). Meandering and transport variations of the Florida Current. *Journal of physical oceanography*, 17(8), 1128-1147, [https://doi.org/10.1175/1520-0485\(1987\)017<1128:MATVOT>2.0.CO;2](https://doi.org/10.1175/1520-0485(1987)017<1128:MATVOT>2.0.CO;2)
- Kang, D. and E. N. Curchitser, 2015. Energetics of eddy-mean flow interactions in the Gulf Stream region, *J. Phys. Oceanogr.*, 45(4): 1103-1120, doi: 10.1175/JPO-D-14-0200.1.
- Kim, S. Y., and G. Crawford (2014), Resonant ocean current responses driven by coastal winds near the critical latitude, *Geophys. Res. Lett.*, 41, 5581–5587, doi:10.1002/2014GL060402.
- Kunze, E., & Toole, J. M. (1997). Tidally driven vorticity, diurnal shear, and turbulence atop Fieberling seamount. *Journal of Physical Oceanography*, 28, 811–814.
- Lee, T. N., and D. A. Mayer (1977). Low-frequency current variability and spin-off eddies on the shelf off southeast Florida, *J. Mar. Res.*, 35(1), 193 – 220.
- Lee, T. N., Atkinson, L. P., and Legeckis, R. (1981). Observations of a Gulf Stream frontal eddy on the Georgia continental shelf, April 1977. *Deep Sea Research Part A. Oceanographic Research Papers*, 28(4), 347-378.
- Lekien, F., and Coulliette, C. (2007). Chaotic stirring in quasi-turbulent flows. *Philosophical Transactions of the Royal Society of London A: Mathematical, Physical and Engineering Sciences*, 365(1861), 3061-3084.
- Mahadevan, A. (2016). The impact of submesoscale physics on primary productivity of plankton. *Annual review of marine science*, 8, 161-184. <https://doi.org/10.1146/annurev-marine-010814-015912>

- Mantovanelli, A., Keating, S. R., Wyatt, L. R., Roughan, M., and Schaeffer, A. (2017). Eulerian and Lagrangian characterization of two counter-rotating submesoscale eddies in a western boundary current. *Journal of Geophysical Research: Oceans*, 122, 4902–4921, doi:10.1002/2016JC011968
- Martinez-Pedraja, J., L. K. Shay, B. K. Haus and C. Whelan, 2013: Interoperability of Sea-sonde and Wellen Radars in mapping surface currents. *J. Atmos. Oceanogr. Tech.*, 30, 2662-2675.
- Mata, M. M., Tomczak, M., Wijffels, S., and Church, J. A. (2000). East Australian Current volume transports at 30 S: Estimates from the World Ocean Circulation Experiment hydrographic sections PR11/P6 and the PCM3 current meter array. *Journal of Geophysical Research: Oceans*, 105(C12), 28509-28526, doi:10.1029/1999JC000121
- McWilliams, J. C. (2016). Submesoscale currents in the ocean. In *Proc. R. Soc. A* (Vol. 472, No. 2189, p. 20160117). The Royal Society. doi:10.1098/rspa.2016.0117
- Meinen, C. S., Baringer, M. O., and Garcia, R. F. (2010). Florida Current transport variability: An analysis of annual and longer-period signals. *Deep Sea Research Part I: Oceanographic Research Papers*, 57(7), 835-846, <https://doi.org/10.1016/j.dsr.2010.04.001>
- Mihanović, H., Pattiaratchi, C., & Verspecht, F. (2016). Diurnal Sea Breezes Force Near-Inertial Waves along Rottneš Continental Shelf, Southwestern Australia. *Journal of Physical Oceanography*, 46(11), 3487-3508.
- Paduan, J. D., and Washburn, L. (2013). High-frequency radar observations of ocean surface currents. *Annual review of marine science*, 5, 115-136, doi: 10.1146/annurev-marine-121211-172315
- Qiu, B. (1999), Seasonal eddy field modulation of the North Pacific Subtropical Countercurrent: TOPEX/Poseidon observations and theory, *J. Phys. Oceaogr.*, **29**, 2471–2486, [https://doi.org/10.1175/1520-0485\(1999\)029<2471:SEFMOT>2.0.CO;2](https://doi.org/10.1175/1520-0485(1999)029<2471:SEFMOT>2.0.CO;2)
- Qiu, B., & Chen, S. (2004). Seasonal modulations in the eddy field of the South Pacific Ocean. *Journal of Physical Oceanography*, 34(7), 1515-1527. [https://doi.org/10.1175/1520-0485\(2004\)034<1515:SMITEF>2.0.CO;2](https://doi.org/10.1175/1520-0485(2004)034<1515:SMITEF>2.0.CO;2)
- Qiu B, Nakano T, Chen S, Klein P, (2017). Submesoscale transition from geostrophic flows to internal waves in the northwestern Pacific upper ocean. *Nature Communications*. 2017;8:14055. doi:10.1038/ncomms14055.
- Richardson, W. S., Schmitz Jr, W. J., and Niiler, P. P. (1969). The velocity structure of the Florida Current from the Straits of Florida to Cape Fear. *Deep-Sea Res*, 16, 225-231.
- Richardson, D. E., Llopiz, J. K., Leaman, K. D., Vertes, P. S., Muller-Karger, F. E., and Cowen, R. K. (2009). Sailfish (*Istiophorus platypterus*) spawning and larval environment in a Florida Current frontal eddy. *Progress in Oceanography*, 82(4), 252-264, <https://doi.org/10.1016/j.pocan.2009.07.003>
- Ridgway, K. R., and Godfrey, J. S. (1997). Seasonal cycle of the East Australian current. *Journal of Geophysical Research: Oceans*, 102(C10), 22921-22936, doi:10.1029/97JC00227
- Rosby, T., and Zhang, H. M. (2001). The near-surface velocity and potential vorticity structure of the Gulf Stream. *Journal of marine research*, 59(6), 949-975.
- Roughan, M., Schaeffer, A., & Suthers, I. M., (2015). Sustained Ocean Observing along the Coast of Southeastern Australia: NSW-IMOS 2007-2014. In: *Coastal Ocean Observing Systems*, Liu, Y., H. Kerkering, R. H. Weisberg, eds. Elsevier. <https://doi.org/10.1016/B978-0-12-802022-7.00006-7>
- Roughan, M., Keating, S. R., Schaeffer, A., Cetina Heredia, P., Rocha, C., Griffin, D., Robertson, R., and Suthers, I. M. (2017). A tale of two eddies: The biophysical characteristics of two contrasting cyclonic eddies in the East Australian Current System. *Journal of Geophysical Research: Oceans*, 122, 2494–2518, doi:10.1002/2016JC012241
- Sasaki, H., Klein, P., Qiu, B., & Sasai, Y. (2014). Impact of oceanic-scale interactions on the seasonal modulation of ocean dynamics by the atmosphere. *Nature communications*, 5, ncomms6636, doi: 10.1038/ncomms6636
- Schaeffer, A., Roughan, M., and Morris, B. D. (2013). Cross-shelf dynamics in a western boundary current regime: Implications for upwelling. *Journal of Physical Oceanography*, 43(5), 1042-1059, <https://doi.org/10.1175/JPO-D-12-0177.1>
- Schaeffer, A., M. Roughan, and J. E. Wood (2014), Observed bottom boundary layer transport and uplift on the continental shelf adjacent to a western boundary current, *J. Geophys. Res. Oceans*, 119, 4922–4939, doi:10.1002/2013JC009735.

- Schaeffer, A., Gramoulle, A., Roughan, M., and Mantovanelli, A. (2017). Characterizing frontal eddies along the East Australian Current from HF radar observations. *Journal of Geophysical Research: Oceans*, 122, 3964–3980, doi:10.1002/2016JC012171
- Schott, F., T.N. Lee, and R. Zantopp, 1988: Variability of structure and transport of the Florida Current in the period range of days to seasonal, *Journal of Physical Oceanography*, 18, 1209-1230, [https://doi.org/10.1175/1520-0485\(1988\)018<1209:VOSATO>2.0.CO;2](https://doi.org/10.1175/1520-0485(1988)018<1209:VOSATO>2.0.CO;2)
- Shay, L. K., T.N Lee, E. J. Williams, H.C. Graber and C. G. H. Rooth (1998), Effects of low frequency current variability on near-inertial submesoscale vortices, *J. Geophys. Res.* 103(C9), 18, 691-18,714.
- Shay, L. K., Cook, T. M., Haus, B. K., Martinez, J., Peters, H., Mariano, A. J., ... and Luther, M. (2000). VHF radar detects oceanic submesoscale vortex along Florida coast. *Eos, Transactions American Geophysical Union*, 81(19), 209-213. <https://doi.org/10.1029/00EO00143>
- Shay, L. K., J. Martinez-Pedraja, T. M. Cook, B. K. Haus, and R. H. Weisberg, 2007: High frequency radar surface current mapping using WERA. *J. Atmos. Oceanogr. Tech.* **24**(3), 484-503.
- Shay LK, Seim H, Savidge D, Styles R, Weisberg RH. 2008. High frequency radar observing systems in SEACOOS: 2002–2007 lessons learned. *Mar. Technol. Soc. J.* 42(3):55–67, <https://doi.org/10.4031/002533208786842435>.
- Shulzitski K, Sponaugle S, Hauff M, Walter K, D’Alessandro EK, Cowen RK. Close encounters with eddies: oceanographic features increase growth of larval reef fishes during their journey to the reef. *Biology Letters*. 2015;11(1):20140746. doi:10.1098/rsbl.2014.0746.
- Simpson, J. H., P. Hyder, T. P. Rippeth, and I. M. Lucas (2002), Forced oscillations near the critical latitude for diurnal-inertial resonance, *J. Phys. Oceanogr.*, 32, 177–187.
- Sloyan, B. M., Ridgway, K. R., and Cowley, R. (2016). The East Australian Current and Property Transport at 27° S from 2012 to 2013. *Journal of Physical Oceanography*, 46(3), 993-1008, <https://doi.org/10.1175/JPO-D-15-0052.1>
- Soh, H. S., and S. Y. Kim (2018), Diagnostic characteristics of submesoscale coastal surface currents, *J. Geophys. Res. Oceans*, 123, doi:10.1002/2017JC013428.
- Szabo, D., & Weatherly, G. L. (1979). Energetics of the Kuroshio south of Japan. *Journal of Marine Research*, 37, 531-556.
- Wyatt, L. R., Mantovanelli, A., Heron, M. L., Roughan, M., & Steinberg, C. R. (2017). Assessment of surface currents measured with high-frequency phased-array radars in two regions of complex circulation. *IEEE Journal of Oceanic Engineering*. doi:10.1109/JOE.2017.2704165
- Xu, Y., & Fu, L. L. (2011). Global variability of the wavenumber spectrum of oceanic mesoscale turbulence. *Journal of physical oceanography*, 41(4), 802-809, <https://doi.org/10.1175/2010JPO4558.1>.
- Yoo, J. G., Kim, S. Y. and Kim, H. S. (2018), Spectral Descriptions of Submesoscale Surface Circulation in a Coastal Region. *J. Geophys. Res. Oceans*. Accepted Author Manuscript. . doi:10.1029/2016JC012517
- Yu, L., & Weller, R. A. (2007). Objectively analyzed air–sea heat fluxes for the global ice-free oceans (1981–2005). *Bulletin of the American Meteorological Society*, 88(4), 527-539, <https://doi.org/10.1175/BAMS-88-4-527>

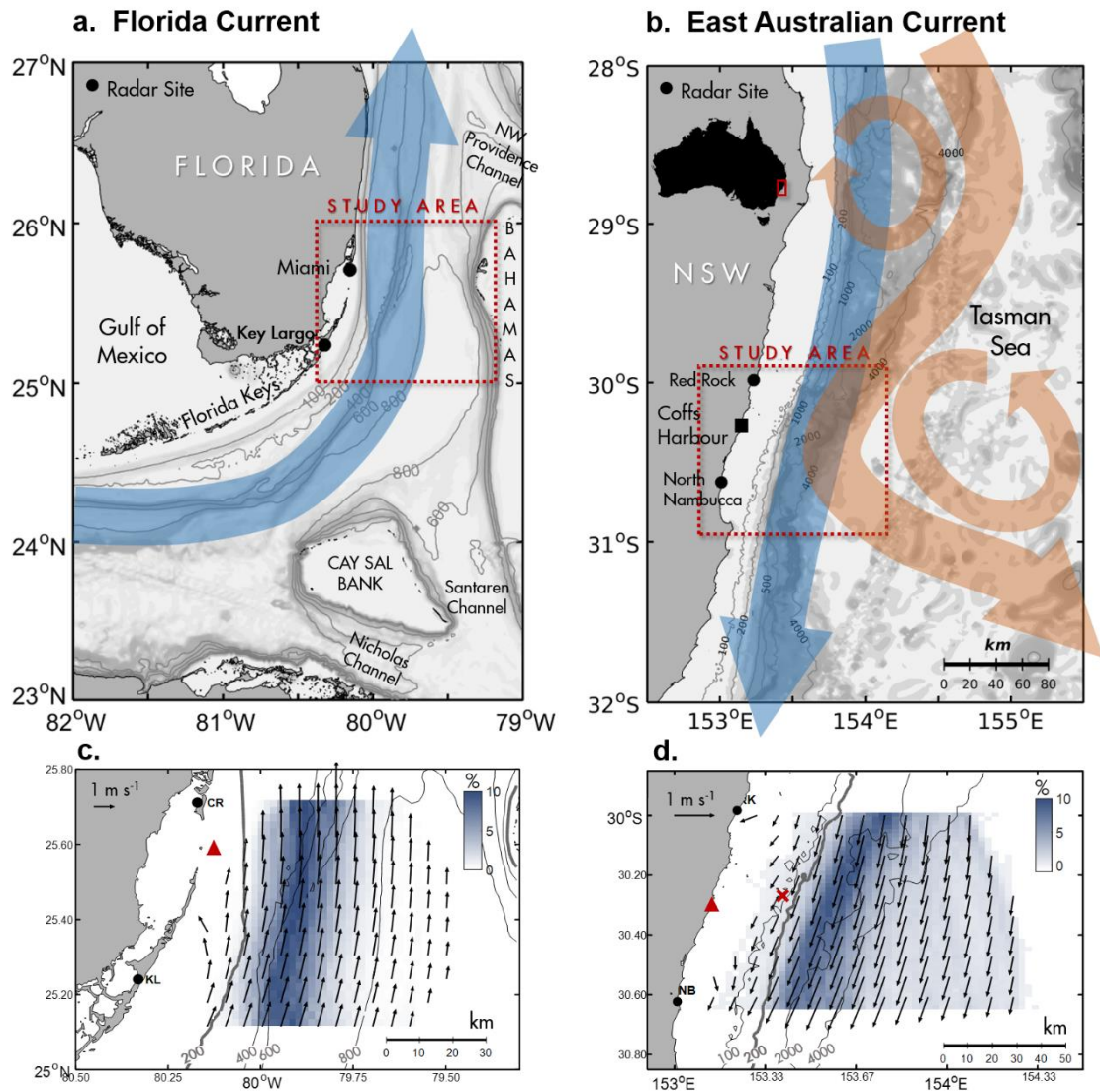


**Fig. 1** Maps of the western boundary current (WBC) systems (a) The Florida Straits (USA), with the Florida Current (FC) in blue. (b) The Tasman Sea offshore New South Wales (NSW), Australia, with the East Australian Current (EAC) in meander mode separating from the shelf (orange) and non-meander (blue). Study areas are depicted with a red-dashed box. (c, d) Mean velocity (black arrows), superimposed on a 2D histogram of jet core location (frequency normalized each latitude to a %), for the FC and EAC, respectively. Red triangles show the wind measurement sites. The red cross in (d) shows the location of mooring CH100. Depth of isobaths is in meters, the thicker gray lines in (c, d) represent the 200 m isobath.

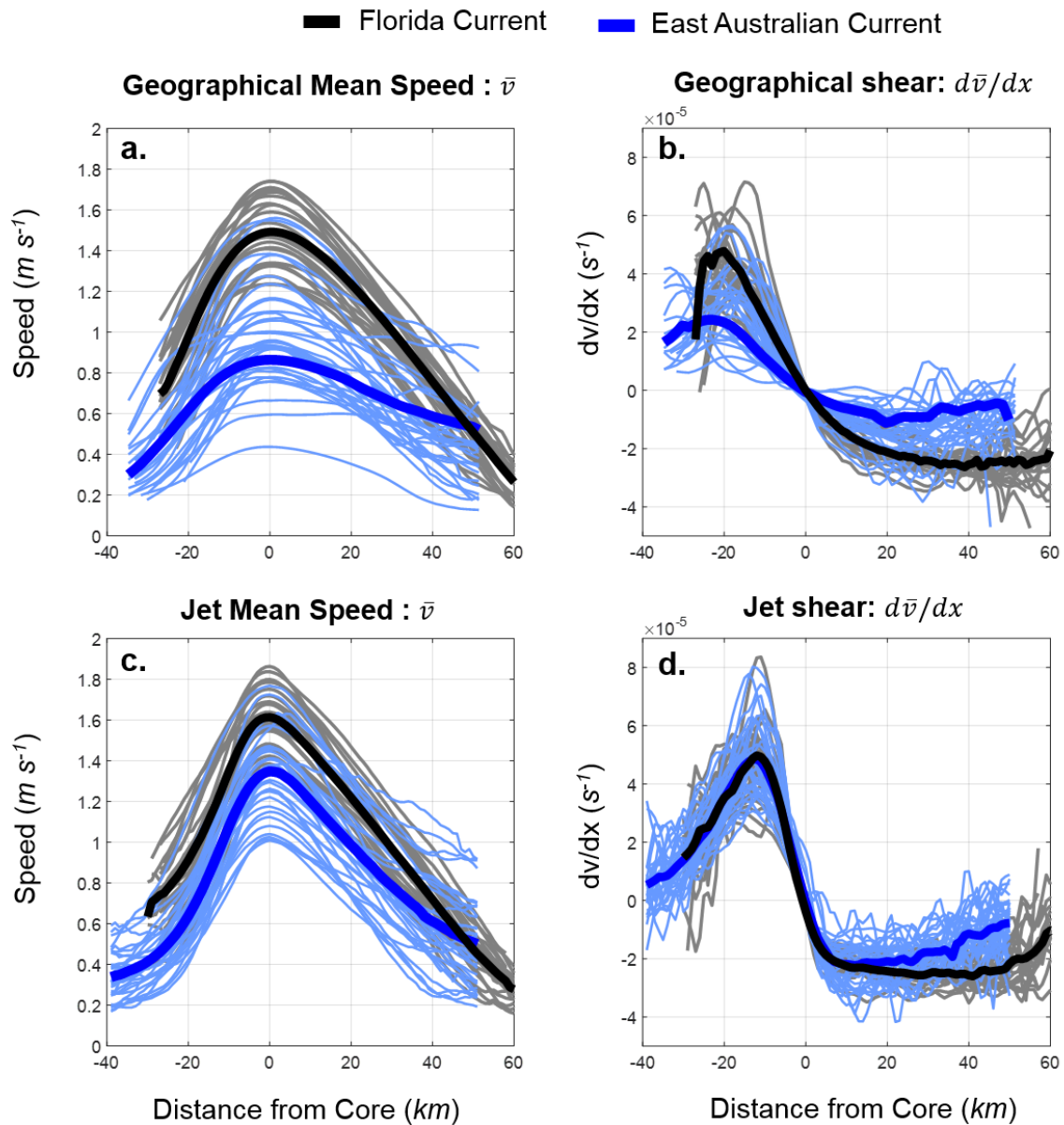


**Fig. 2 Time-mean across-jet profiles of speed and lateral shear** (a) Geographical coordinate frame speed; (b) Geographical shear; (c) Jet coordinate frame speed; (d) Jet shear. Thin lines represent all monthly averages for the observation periods; thick lines represent the total time mean.

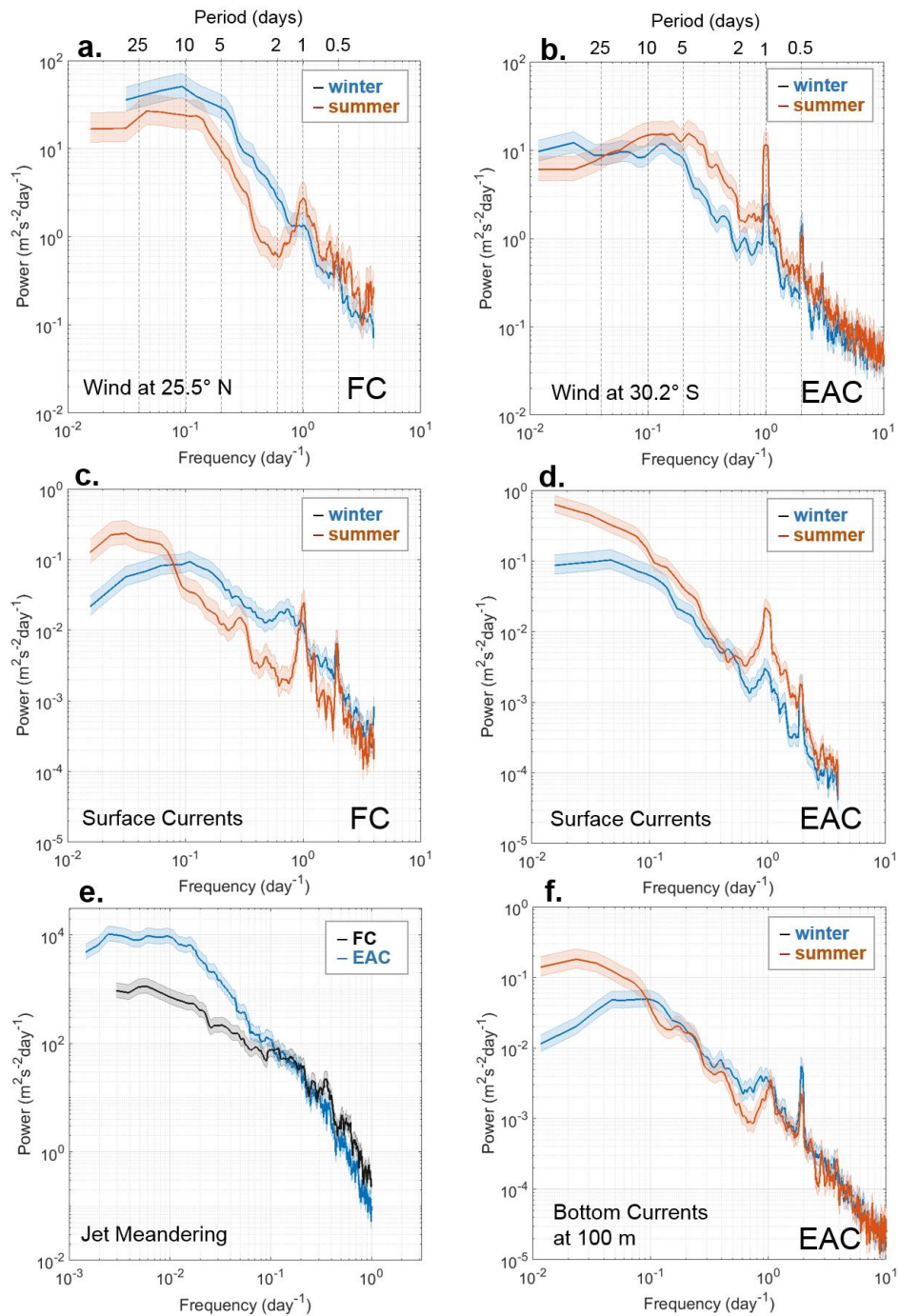


**Fig. 3 Kinetic energy frequency power spectra** (a) Wind at 25.5° N off Miami, FL; (b) Wind at 30.2° S at Coffs Harbour; (c) FC surface currents at grid cell 25.36°N, 80.02°W; (d) EAC surface currents at grid cell 31.31°S, 153.19°E corresponding to mooring CH100; (e) FC and EAC meandering time series; (f) Mooring CH100 bottom currents at 100 m isobath (measured at 89 m). Shading denotes 95% confidence intervals.

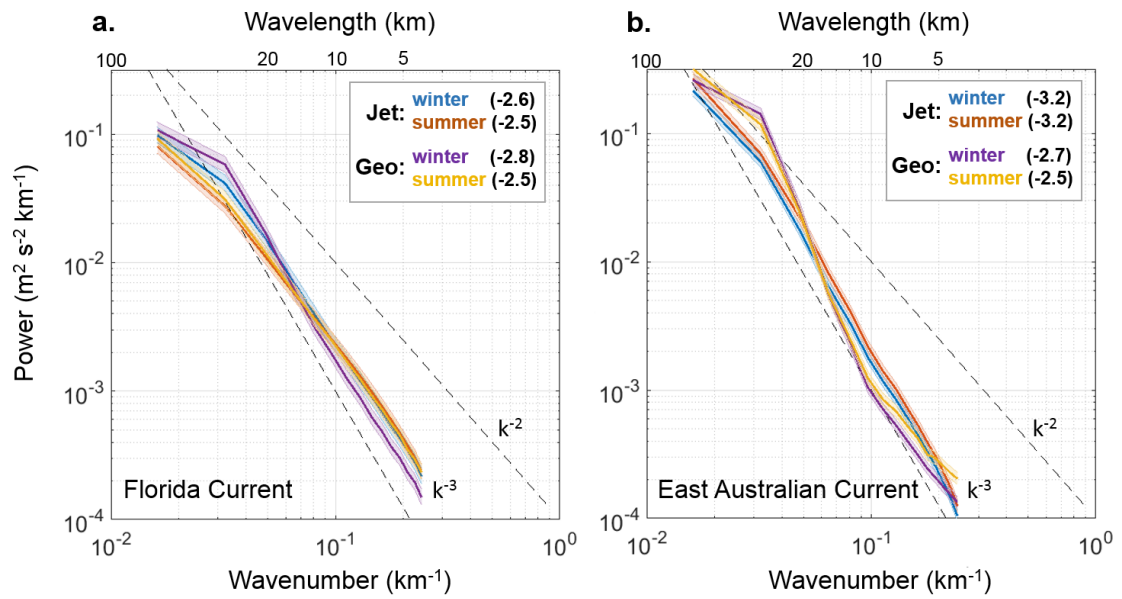


**Fig. 4 Eddy kinetic energy 1D wavenumber power spectra** Numbers in parentheses denote the mean slope of the line across all wavenumbers. Shading denotes 95% confidence intervals.